

Article

CuO-In₂O₃ Catalysts Supported on Halloysite Nanotubes for CO₂ Hydrogenation to Dimethyl Ether

Alexey Pechenkin ^{1,2,*}, Dmitry Potemkin ^{2,3} , Maria Rubtsova ¹ , Pavel Snytnikov ² , Pavel Plyusnin ⁴ 
and Aleksandr Glotov ¹ 

¹ Department of Physical and Colloid Chemistry, Faculty of Chemical Technology and Ecology, Gubkin Russian State University of Oil and Gas, 65 Leninsky prosp., 119991 Moscow, Russia; artemovamai@gmail.com (M.R.); glotov.a@gubkin.ru (A.G.)

² Borskov Institute of Catalysis, Pr. Akademika Lavrentieva, 5, 630090 Novosibirsk, Russia; potema@catalysis.ru (D.P.); pvsnyt@catalysis.ru (P.S.)

³ Department of Environmental Engineering, Novosibirsk State Technical University, Karl Marx Pr., 20, 630073 Novosibirsk, Russia

⁴ Nikolaev Institute of Inorganic Chemistry, Siberian Branch of the Russian Academy of Science, 630090 Novosibirsk, Russia; plus@niic.nsc.ru

* Correspondence: pechenkin@catalysis.ru

Abstract: Hydrogenation of CO₂ relative to valuable chemical compounds such as methanol or dimethyl ether (DME) is an attractive route for reducing CO₂ emissions in the atmosphere. In the present work, the hydrogenation of CO₂ into DME over CuO-In₂O₃, supported on halloysite nanotubes (HNT) was investigated in the temperature range 200–300 °C at 40 atm. HNT appears to be novel promising support for bifunctional catalysts due to its thermal stability and the presence of acidic sites on its surface. CuO-In₂O₃/HNT catalysts demonstrate higher CO₂ conversion and DME selectivity compared to non-indium CuO/HNT catalysts. The catalysts were investigated by N₂ adsorption, X-ray diffraction, hydrogen-temperature programmed reduction and transition electron microscopy. The acid sites were analyzed by temperature programmed desorption of ammonia. It was shown that CuO/HNT was unstable under reaction conditions in contrast to CuO-In₂O₃/HNT. The best CuO-In₂O₃/HNT catalyst provided CO₂ conversion of 7.6% with 65% DME selectivity under P = 40 atm, T = 250 °C, gas hour space velocity 12,000 h⁻¹ and H₂:CO₂ = 3:1.

Keywords: CO₂ hydrogenation; dimethyl ether; indium oxide; copper-indium catalysts; halloysite nanotubes; aluminosilicates



Citation: Pechenkin, A.; Potemkin, D.; Rubtsova, M.; Snytnikov, P.; Plyusnin, P.; Glotov, A. CuO-In₂O₃ Catalysts Supported on Halloysite Nanotubes for CO₂ Hydrogenation to Dimethyl Ether. *Catalysts* **2021**, *11*, 1151. <https://doi.org/10.3390/catal11101151>

Academic Editor:
Hamidreza Arandiyani

Received: 22 August 2021
Accepted: 24 September 2021
Published: 25 September 2021

Publisher's Note: MDPI stays neutral with regard to jurisdictional claims in published maps and institutional affiliations.



Copyright: © 2021 by the authors. Licensee MDPI, Basel, Switzerland. This article is an open access article distributed under the terms and conditions of the Creative Commons Attribution (CC BY) license (<https://creativecommons.org/licenses/by/4.0/>).

1. Introduction

Currently, global warming is considered as one of the global environmental concerns along with air pollution. One of the reasons for these problems is the ever-increasing emissions of CO₂ in the atmosphere as a result of various industrial factories. In order to address these issues, researchers are developing new methods to efficiently convert carbon dioxide into valuable chemical materials. One of these methods include the hydrogenation of CO₂ to methanol or dimethyl ether (DME) [1]. The direct synthesis of DME is more favorable than methanol due to thermodynamics [2], higher H/C ratio and non-toxicity. The dimethyl ether (DME) is one of the most important chemicals due to its properties and application in various fields. DME is also considered as an alternative “green” fuel because its properties are similar to liquefied petroleum gas (LPG); therefore, it can be easily stored and transported by using the existing infrastructure for LPG [3,4]. DME is used as a precursor in organic synthesis for the production of diethyl sulfate, methyl acetate or olefins [5] as a solvent and as an aerosol for various personal care products [6]. Furthermore, DME can be used as a hydrogen source for low-temperature proton-exchange membrane fuel cells by autothermal or steam reforming [7]. Moreover, DME is an alternative to

diesel fuel due to its similar cetane number, lower emissions of soot particles and NO_x in exhaust gases [8].

Currently, the process of DME production can be carried out with two methods: The first is an indirect route using two reactors with methanol synthesis on a metallic copper-based catalyst, and it involves dehydration to DME over solid acid catalysts. This is an industrial process. The second method is the direct synthesis of DME from CO₂ in a single reactor using bifunctional catalyst consisting of two types of active sites—metallic for methanol synthesis and acid sites for methanol dehydration [9]. The direct synthesis process has some advantages in comparison with the traditional one: first, higher conversion of reactants results from the removal of thermodynamic restrictions; and second, using a single reactor results in lower DME production costs. The direct synthesis of DME by CO₂ hydrogenation involves three reactions: methanol synthesis from CO₂ and H₂ (1), dehydration of formed methanol to DME (2) and side reaction and reverse water gas shift reaction (3).



As mentioned above, this scheme requires two types of active sites on the catalysts' surface: the first type involves metal particles to methanol synthesis; and the second type involves acid sites for methanol dehydration to DME. Moreover, the catalyst has to be inactive in undesirable CO₂ methanation and methanol/DME condensation reactions.

In recent years, In₂O₃ was viewed as a promising catalyst for the synthesis of methanol from CO₂ due to its excellent selectivity for methanol in the temperature range 200–320 °C [10–12]. Using a density functional theory, Ye et al. [10] demonstrated that defective In₂O₃ had great performance in CO₂ hydrogenation. It was shown that methanol synthesis on defective In₂O₃ was followed by a mechanism including the cycling reaction of activated CO₂ molecules on oxygen vacancies. After that, many researchers investigated the catalytic properties of indium oxide in methanol synthesis reaction [11–15]. In the work by Sun et al. [11], pure In₂O₃ was used as a catalyst in methanol synthesis from CO₂. This catalyst shows low CO₂ conversion (1.1%) with 54.9% methanol selectivity at 270 °C and 40 atm. However, by increasing temperatures up to 330 °C, CO₂ conversion rises to 7.1%, since methanol selectivity decreases to 39.7%. This value of selectivity at this temperature is quite high, which is associated with the inhibition of RWGS reaction. Martin et al. [12] reported that In₂O₃/ZrO₂ exhibited 5.2% CO₂ conversion with 99.8% methanol selectivity at 300 °C, 50 atm and H₂:CO₂ = 4:1. The next step in the study of the catalytic activity of indium-based catalysts was with Pd/In₂O₃ catalysts. Rui et al. [14] showed that Pd-P/In₂O₃ catalyst had great results in CO₂ hydrogenation to methanol—above 20% CO₂ conversion and above 70% selectivity for methanol at 300 °C and 50 atm. Nevertheless, Pd is quite expensive, which leads to finding low-cost and efficient catalysts for methanol synthesis by CO₂ hydrogenation.

Up to this point, Cu-based catalysts are typically used as catalysts for methanol synthesis [16–22]. Many various promoters have been investigated in order to improve the catalytic properties of copper catalysts. The most popular catalysts with promoters are CuO-ZnO-Al₂O₃ [16,17], CuO-ZnO-Al₂O₃-ZrO₂ [18,19] and CuO-ZnO-ZrO₂ [20–22]. However, with the growing interest in indium oxide as a catalyst for methanol synthesis, some investigations devoted to the study of copper-indium catalysts appeared. For example, Shi Z. et al. [23] investigated a CuIn@SiO₂ core-shell catalyst prepared by the solvothermal method for CO₂ hydrogenation to methanol with 9.8% CO₂ conversion and 78.1% methanol selectivity at 280 °C and 30 atm. Yao et al. [24] have examined the Cu-In-Zr-O mixed oxide catalysts in methanol synthesis. The catalytic activity of this sample was 1.48% CO₂ conversion with 79.7% methanol selectivity at 250 °C and 25 atm. In this work, we report CO₂ hydrogenation to DME by using CuO-In₂O₃ oxides as a methanol synthesis component.

Halloysite nanotubes (HNT) are one of the promising materials used as a catalysts support, which has recently attracted great interest from researchers [25]. HNT is a natural aluminosilicate of the kaolin group, with a hollow tubular structure 1–1.5 μm in length, ca. 50 nm in outer diameter and 10–15 nm in terms of inner diameter. The outer surface of HNT is formed from alumina and negatively charged, while the inner is formed from silica with a positive charge. These unique features of HNT possess selective modification of outer/inner surfaces by metals (Au, Ag, Ru, Pd, Cu, Pt, etc.) or organics in order to adjust morphology and to tune catalytic properties [26–28]. In recent years, research study focuses shifted towards the design and development of functional materials based on HNT for coatings, drug delivery, fabrication of high-quality ceramics and catalysis [29–31]. Compared to synthetic aluminosilicates such as zeolites, mesoporous silicas, alumina or carbon nanotubes, HNT is a low-cost clay material that is abundantly available, safe and environment-friendly [32–36]. It is characterized by high mechanical strength (above 500 MPa) and possesses up to 1100 $^{\circ}\text{C}$ thermal stability [35]. After heating above 400–450 $^{\circ}\text{C}$, the halloysite rolled structure loses water molecules incorporated into the interlayer cavity [35].

A combination of copper-indium catalyst as a metallic component with HNT as an acidic component will make obtaining a highly effective catalyst for direct CO_2 hydrogenation to DME possible.

In the present work, we report the synthesis, catalytic activity and structural characterization of novel copper and copper-indium catalysts, supported on HNT in CO_2 hydrogenation to DME.

2. Results

Characterization of Catalysts

Fresh and used CuO/HNT and $\text{CuO-In}_2\text{O}_3/\text{HNT}$ catalysts were studied by several methods, such as XRD, S_{BET} , NH_3 -TPD and inductively coupled plasma atomic emission spectroscopy (ICP-AES). The summarized data are presented in Table 1. Metal loadings, obtained by ICP-AES, are similar to fresh and used CuO/HNT and $\text{CuO-In}_2\text{O}_3/\text{HNT}$ catalysts; thus, there is no metal loss during the reaction. Real copper and indium loadings are slightly lower than the calculated ones (10 wt.% for both metals) since some experimental errors, due to a larger amount of crystalline water in precursors, appeared to contrast those given in the datasheet. Moreover, S_{BET} did not change during CO_2 hydrogenation in the case of both catalysts. The BET surface area of CuO/HNT is 62 m^2/g and is lower than 71 m^2/g for pure HNT. A similar behavior was observed for $\text{CuO-In}_2\text{O}_3/\text{HNT}$, for which its S_{BET} is 55 m^2/g . The acidity parameters of the catalysts and supports calculated from NH_3 -TPD method are listed in Table 1. Nitrogen adsorption/desorption isotherms and pore size distribution of $\text{CuO-In}_2\text{O}_3/\text{HNT}$ catalyst are presented in Supplementary Materials (Figure S1). Based on the desorption spectra, acidity was classified as weak and medium (amount of ammonia ($\mu\text{mol}/\text{g}$) desorbed below 300 $^{\circ}\text{C}$) and strong sites (amount of ammonia ($\mu\text{mol}/\text{g}$) desorbed above 300 $^{\circ}\text{C}$). As shown in Table 2, the acidity of supported catalysts is slightly lower than that of the pure halloysite. This is explained by some metal particles blocking surface acid sites, which results in a decrease in their amount.

Table 1. Physical-chemical properties of HNT, CuO/HNT and $\text{CuO-In}_2\text{O}_3/\text{HNT}$.

Catalyst	Metal Loading, wt.%		Acidity Sites, $\mu\text{mol}/\text{g}$			S_{BET} , m^2/g
	Cu	In	Weak and Medium *	Strong **	Total Amount	
HNT	-	-	22	122	144	71
CuO/HNT	fresh	9.7	-	18	110	62
	used	9.7	-	18	110	62
$\text{CuO-In}_2\text{O}_3/\text{HNT}$	fresh	9.8	9.4	15	99	114
	used	9.8	9.4	15	99	114

* Amount of ammonia desorbed below 300 $^{\circ}\text{C}$. ** Amount of ammonia desorbed above 300 $^{\circ}\text{C}$.

Table 2. XRD data for the CuO/HNT and CuO-In₂O₃/HNT catalysts.

Catalyst		Unit Cell Parameters, nm		CSR, nm	
		a (In ₂ O ₃)		D (Cu)	D (In ₂ O ₃)
CuO/HNT	fresh	-		15	-
	used	-		59	-
CuO-In ₂ O ₃ /HNT	fresh	1.0054		-	8
	used	1.0089		8.5	8

The catalysts were examined by X-ray diffraction analysis. The results are shown in Figure 1. According to XRD patterns (Figure 1a) of HNT, fresh CuO/HNT and CuO-In₂O₃/HNT catalysts have peaks correlated with copper (II) oxide (PDF# 00-005-0661, $a = 4.684 \text{ \AA}$, $b = 3.425 \text{ \AA}$, $c = 5.129 \text{ \AA}$ and $\beta = 99.47^\circ$) with a crystallite size of 15 nm. The XRD pattern of used CuO/HNT contained peaks of metal copper particles (PDF# 00-004-0836, $a = b = c = 3.615 \text{ \AA}$) with a crystallite size of 59 nm. This is explained by the fact that the catalyst is in a reducing atmosphere during the CO₂ hydrogenation reaction to DME. The observed significant increase in copper crystallite size indicates that copper particles on the HNT surface are sintered into larger agglomerates during the reaction. In the case of a used copper-indium catalyst, different results are observed. On XRD patterns, we can see peaks of indium oxide (PDF# 00-006-0416, $a = b = c = 10.110 \text{ \AA}$, crystallite size 8 nm) and metallic copper (PDF# 00-004-0836, $a = b = c = 3.615 \text{ \AA}$, crystallite size 13 nm).

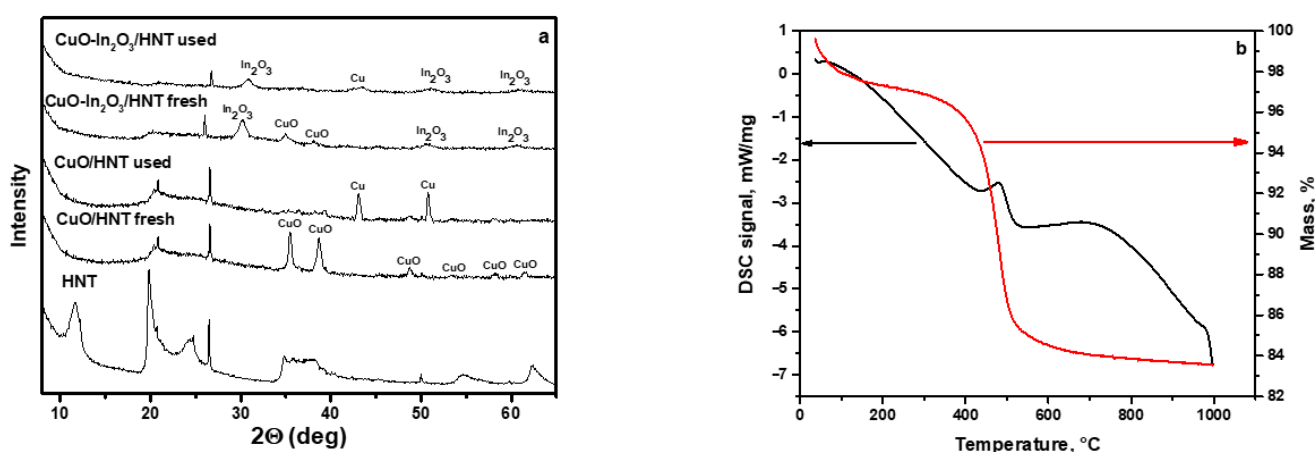


Figure 1. (a) XRD patterns of HNT, CuO/HNT and CuO-In₂O₃/HNT catalysts. (b) Thermogravimetric analysis (TGA) curve for pristine HNT.

The unit cell parameter of indium oxide 1.0054 nm is lower than the standard bulk value $1.1011 (\pm 0.003 \text{ \AA}) \text{ nm}$ [37]. This is most likely due to the insertion of Cu²⁺ (ion radius 0.73 Å) cations into In₂O₃ (ion radius 0.80 Å) lattice. As observed from the XRD pattern of the used CuO-In₂O₃/HNT catalyst, there are peaks correlated with phases of Cu and In₂O₃. Note that the unit cell parameter of In₂O₃ slightly increases to 1.0089 nm, but it is still lower than the bulk value. A decrease in the intensity of peaks from the In₂O₃ phase, an increase in the intensity of peaks from copper-containing phases and an increase in the lattice parameter of In₂O₃ indicates a partial release of copper from the mixed oxide composition. By summarizing all data, we can conclude that the active sites of this catalyst are indium oxide particles mixed with copper particles. Furthermore, the addition of indium oxide to copper catalysts results in copper particles stabilizing on the surface of the catalyst, and its sintering is suppressed. The absence of HNT-related peaks on XRD patterns for samples with immobilized metal oxides could be assigned to interlayer water molecules loss after calcination during the catalyst preparation step (Figure 1b, Figures S2 and S3) [35]. Meanwhile, the retention of the tubular structure of

HNT is observed from TEM images (Figure 2), and its thermal stability up to 1000 °C was confirmed by TGA analysis (Figure 1b).

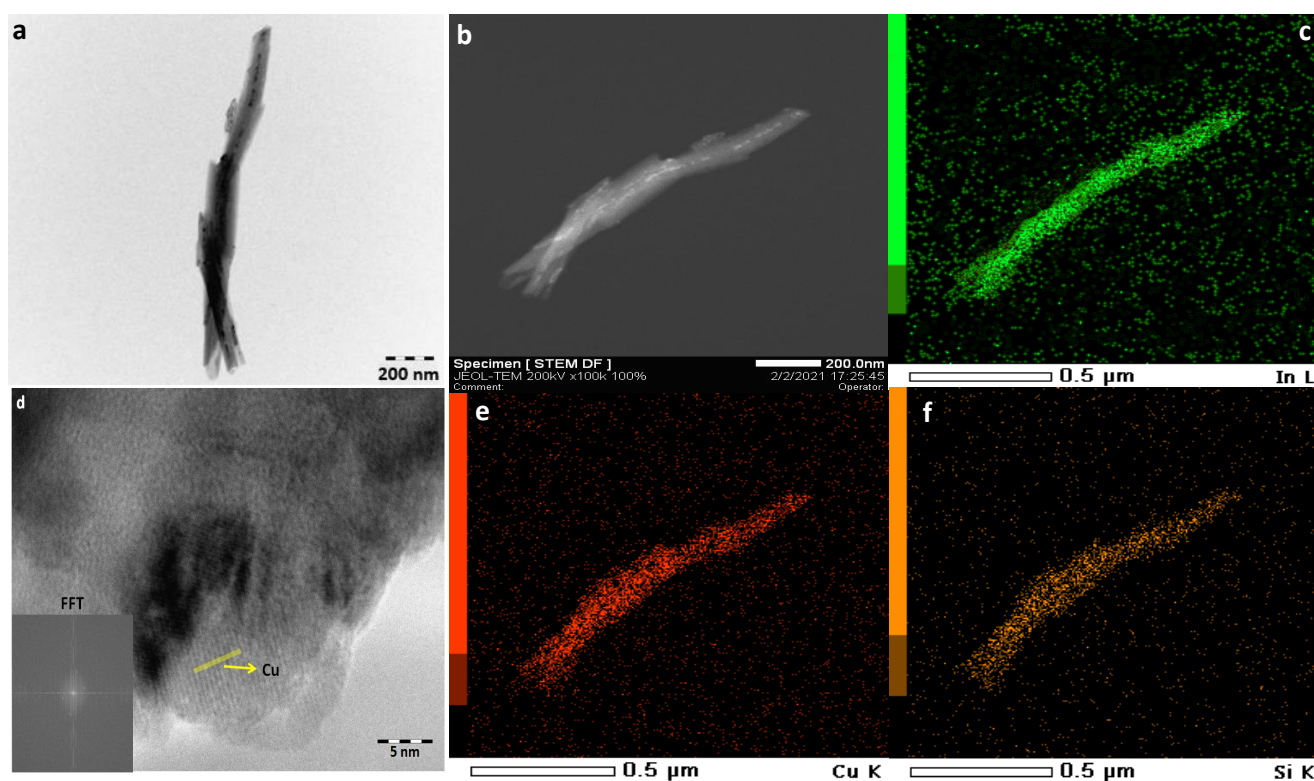


Figure 2. TEM (a,d) and STEM (b) images and EDX-mapping (c,e,f) of used CuO-In₂O₃/HNT catalyst.

Figure 2 shows TEM images of the used CuO-In₂O₃/HNT catalyst and element distribution in this catalyst. We can observe that all elements are distributed uniformly on the catalyst's surface (Figure 2c,e,f). Halloysite nanotubes were observed in both samples, and the images show that the nanotubes remained stable under reaction conditions. On HR TEM, we can only observe the copper particles according to interplanar distance. In accordance with XRD data for used catalyst, we can observe that the indium particles are located mainly in the same locations as the silicon and copper particles in the case of both catalysts from the elemental mapping. Thus, it can be concluded that CuO-In₂O₃/HNT catalyst contains two types of active sites on the surface: copper particles mixed with indium oxide particles supported on silica, which are responsible for methanol synthesis, and alumina oxide particles, which are responsible for methanol dehydration.

Figure 3 shows the reducibility of fresh CuO/HNT and CuO-In₂O₃/HNT catalysts investigated by the H₂-TPR method. It should be noted that indium oxide does not reduce in the investigated temperature range. In the case of CuO/HNT, we can observe two peaks of hydrogen uptake—at 225 and 245 °C. This fact can be explained by the reduction in small and large copper particles [38] on the catalyst surface. At the same time, for the CuO-In₂O₃/HNT catalyst, only one peak at 230 °C was observed on the graph. It can be attributed to the absence of large copper particles on the catalyst surface.

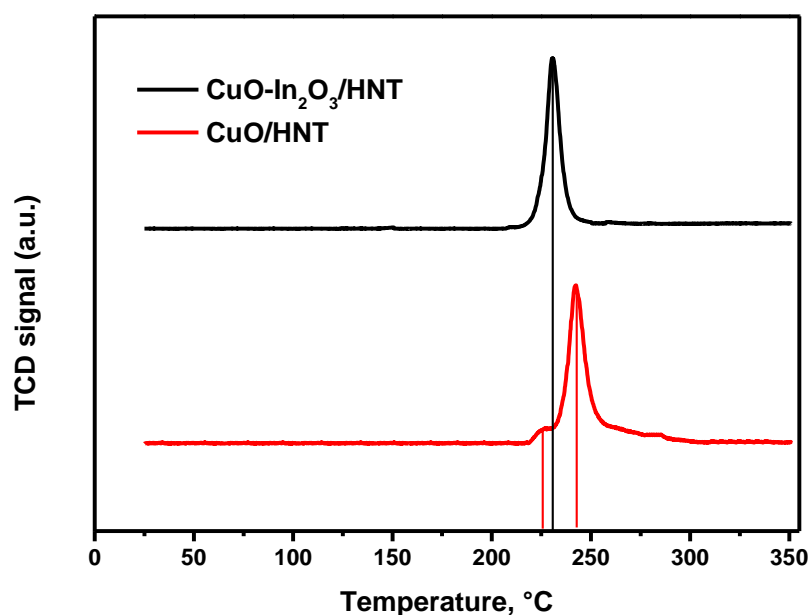


Figure 3. H₂-TPR profiles of CuO/HNT and CuO-In₂O₃/HNT catalysts.

The results obtained allow us to conclude that there are two types of active sites on the catalyst surface: metal particles (copper for CuO/HNT and copper-indium for CuO-In₂O₃/HNT) for methanol synthesis and acidic sites of HNT for dehydration of methanol to DME.

The catalytic properties of CuO/HNT and CuO-In₂O₃/HNT catalysts were studied in CO₂ hydrogenation to DME. The reaction conditions were T = 200–300 °C, P = 40 atm and GHSV = 12,000 h⁻¹ (V_{cat} = 2 mL, m_{cat} ~1.2 g). Only CO, H₂O, methanol and dimethyl ethers were detected as reaction products. No hydrocarbons were observed in the products. Figure 4 shows the temperature dependencies of CO₂ conversion, CO and DME selectivity for CO₂ hydrogenation to DME over CuO/HNT and CuO-In₂O₃/HNT catalysts. We can observe that CO₂ conversion is almost similar for both catalysts, but the values of DME selectivity are higher on CuO-In₂O₃/HNT than that on CuO/HNT. This is most likely connected with the fact that the reverse water gas shift reaction on CuO/HNT is not suppressed, unlike CuO-In₂O₃/HNT [10]. This is confirmed by CO selectivity on these catalysts, which is higher on CuO/HNT.

As we can observe from the graph, CO₂ conversion increases with increasing temperature, while DME selectivity, on contrary, decreases. Such behavior is consistent with thermodynamic data: The dehydration of methanol is an exothermic reaction; thus, the evolving reaction heat results in a decrease in DME formation rates. Following this, the temperature dependence of the DME production rate is also explained. The results are shown in Figure 5.

The DME production rate passes through the maximum at 250 °C and then decreases despite the increase in CO₂ conversion. The maximum of DME production rates reaches 0.203 g_{DME}/g_{cat}·h over CuO-In₂O₃/HNT at 40 atm, T = 250 °C, GHSV = 12,000 h⁻¹ and inlet composition of H₂:CO₂ = 3:1.

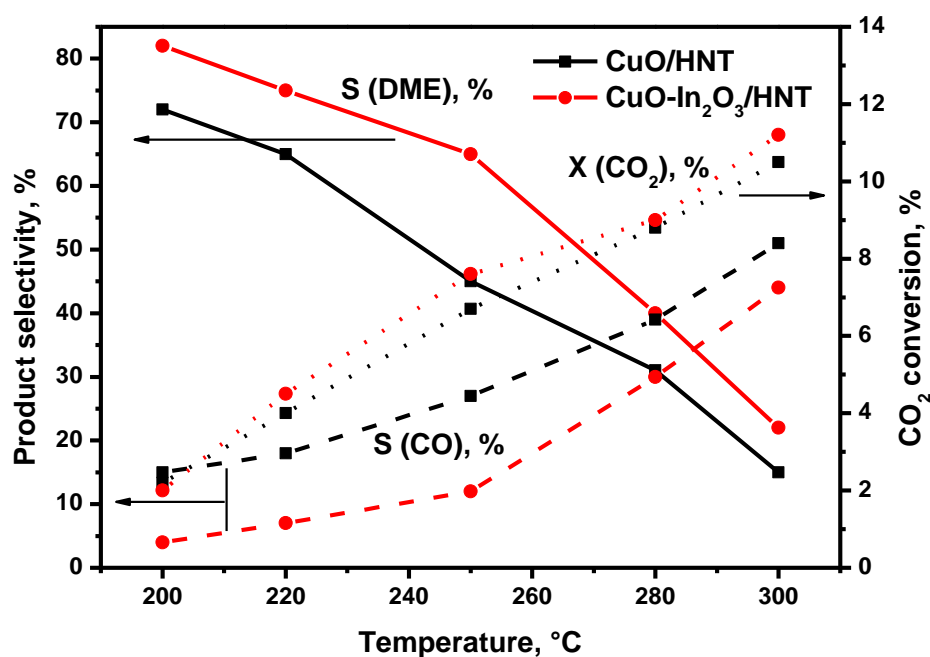


Figure 4. Effect of temperature on CO₂ conversion, CO and DME selectivity over CuO/HNT and CuO-In₂O₃/HNT catalysts. Reaction conditions: P = 40 atm, GHSV = 12,000 h⁻¹; Inlet composition, vol.%: H₂:CO₂ = 3:1.

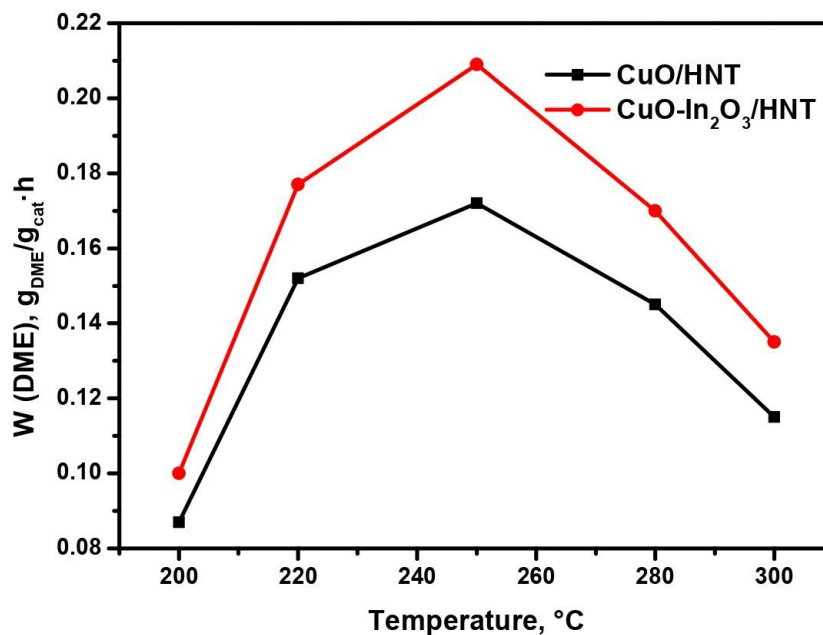


Figure 5. Effect of temperature on DME production rate over CuO/HNT and CuO-In₂O₃/HNT catalysts. Reaction conditions: P = 40 atm, GHSV = 12,000 h⁻¹; Inlet composition, vol.%: H₂:CO₂ = 3:1.

It is well known that copper catalysts suffer from deactivation problems due to sintering [39]. In order to solve this problem, promoters are usually added to catalysts to increase the stability of the copper particles. A series of experiments was carried out to study the effect of indium oxide particles on the stability of the surface copper particles. Figure 6 presents CO₂ conversion and DME selectivity as a function of a time on stream for CO₂ hydrogenation at 250 °C over CuO/HNT and CuO-In₂O₃/HNT catalysts. As we can observe from Figure 6, CO₂ conversion and DME selectivity were constant in the case of CuO-In₂O₃/HNT and decreased with time for CuO/HNT. According to TPO experiments,

no coke formation for both catalysts was observed. Thus, from our point of view and by considering the XRD data, the most likely reason for CuO/HNT deactivation is the sintering of copper particles during the reaction.

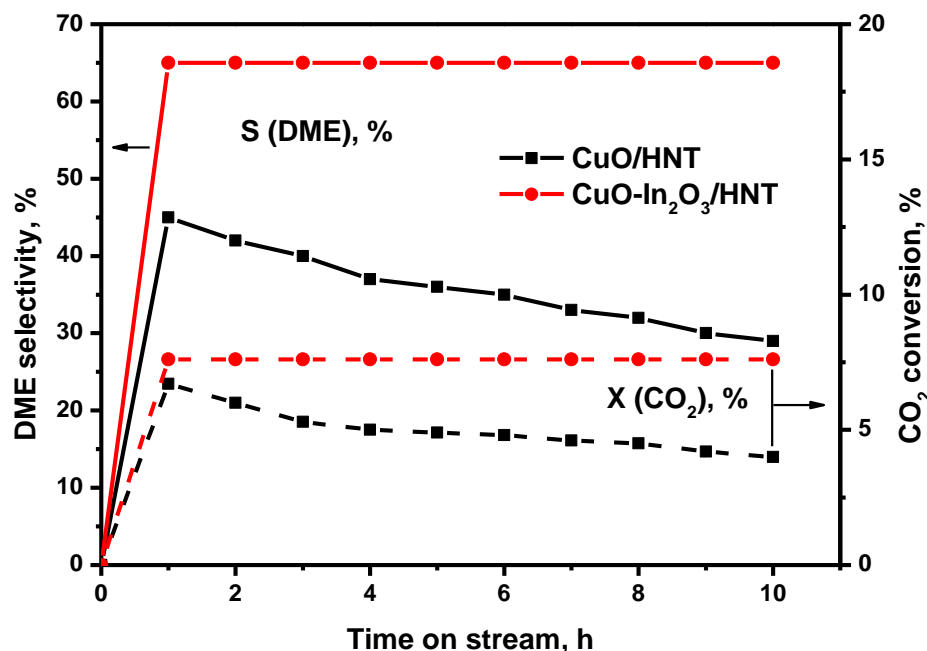


Figure 6. Effect of time on stream on CO₂ conversion and DME selectivity over CuO/HNT and CuO-In₂O₃/HNT catalyst. Reaction conditions: T = 250 °C, P = 40 atm and GHSV = 12,000 h⁻¹; Inlet composition, vol.%: H₂:CO₂ = 3:1.

Thus, CuO-In₂O₃/HNT showed sufficient activity in CO₂ hydrogenation to DME at 40 atm and T = 250 °C. This fact was attributed to the stability and activity of copper and indium oxide particles in the synthesis of methanol and the stability and activity of acid sites of HNT in further methanol dehydration. The catalytic activity of CuO-In₂O₃/HNT could be improved further by optimizing metal loading, modifying HNT or balancing reaction conditions.

Indium oxide-based catalysts for methanol synthesis have only recently gained popularity, and the investigations are still at an early stage. Most of the work on indium catalysts is devoted to the synthesis of methanol [10–15], while only one article on the synthesis of DME has been published so far [40]. Therefore, it is a point of interest to compare the activity of new copper-indium catalysts and systems well studied in the literature. Table 3 shows comparative data.

Table 3. Comparison of catalyst activities in CO₂ hydrogenation to dimethyl ether.

Catalyst	T, °C	Pressure, atm	GHSV, mL/g _{cat} ·h	S (DME), %	W (DME), gDME/g _{cat} ·h	Reference
CuO-In ₂ O ₃ /HNT	250	40	12,000	65	0.203	This work
CIZO ¹ /SAPO-34	250	30	6000	65.1	0.08	[40]
CZA ² /H-ZSM-5	240	30	452	69	0.27	[18]
CZA/HZSM-5	260	50	3000	65	0.29	[19]
CZZ ³ /ferrierite	260	50	8800	40	0.435	[20]
CZZ/H-ZSM-5	240	30	2200	49	0.251	[21]
CZZ/beta	260	30	8800	30	0.3	[22]

¹ CuO-In₂O₃-ZrO₂. ² CuO-ZnO-Al₂O₃. ³ CuO-ZnO-ZrO₂.

We can observe that, compared to state-of-art catalysts, our catalyst shows excellent performance in the case of DME selectivity, which is the key reason for using indium oxide catalysts. Compared to Cu-In-Zr-O catalysts admixed with SAPO-34, the CuO-In₂O₃/HNT catalyst shows the same DME selectivity but higher CO₂ conversion, which results in an increase in DME productivity. However, at the same time, both CO₂ conversion and DME productivities are lower compared with common CZZ or CZA catalysts. As described in the literature [10], indium oxide inhibits RWGS reaction, and catalysts with indium oxide can operate at higher temperatures with lower CO selectivity compared to traditional copper-based catalysts. These copper-indium systems look very promising in the field of direct DME synthesis by CO₂ hydrogenation but require further investigation.

3. Materials and Methods

Aluminosilicate halloysite nanotubes (Al₂Si₂O₅(OH)₄) (Sigma-Aldrich, St. Louis, MO, USA) were used as supports for catalysts.

CuO/HNT and CuO-In₂O₃/HNT were prepared by incipient wetness impregnation. HNT was impregnated with a solution of copper (II) nitrate to obtain 10 wt.% CuO/HNT. In the case of 10 wt.% CuO-10 wt.% In₂O₃/HNT catalyst, a combined solution of copper (II) and indium (III) nitrates was used for impregnation. The samples were dried at 80 °C in the air for 4 h, and they were calcined at 450 °C (heating rate 1 °C/min) for 3 h in air after.

The fresh and used catalysts were characterized by transmission electron microscopy (TEM), EDX-mapping, X-ray powder diffraction (XRD), low-temperature nitrogen adsorption (S_{BET}), temperature-programmed desorption of ammonia (NH₃-TPD), inductively coupled plasma atomic emission spectrometry (ICP-AES) and temperature-programmed oxidation (TPO) methods.

Transmission electron microscopy images of the samples were obtained using a JEOL JEM-2100 (UHR) (Jeol Ltd.; Tokyo, Japan) operated at 200 kV (the lattice resolution of 0.19 nm) equipped with a LaB₆ gun. The catalysts for the TEM analysis were dispersed in ethanol and, after that, dropped into a carbon-coated formvar TEM Cu grid (300 mesh, Ted Pella, Inc.). The acquisition of TEM/HRTEM images was performed in TEM mode by using an Olympus Quemesa 11-megapixel CCD camera (Tokyo, Japan). The analysis of structure, morphology and chemical composition of the supported particles was performed by using an EX-24065JGT energy dispersive X-ray (EDX) analyzer (Jeol Ltd.; Tokyo, Japan) in STEM mode.

The specific BET surface areas (S_{BET}) of the samples were determined from low-temperature nitrogen adsorption isotherms by using a TriStar3000 apparatus (Micromeritics, Norcross, GA, USA). Before the experiment, all samples were outgassed in a vacuum at 300 °C; then, nitrogen adsorption/desorption isotherms were recorded at -196 °C. The specific surface area of the samples was calculated by the Brunauer–Emmett–Teller (BET) equation. The pore volume was evaluated by using the Barrett–Joyner–Halenda model.

Total acidities of CuO/HNT and CuO-In₂O₃/HNT catalysts were calculated by using a temperature-programmed desorption of ammonia (NH₃-TPD) on a Micromeritics AutoChem HP2950 apparatus (Micromeritics, Norcross, GA, USA). First, the catalyst was held in a stream of nitrogen at 300 °C for 1 h. After that, the sample was saturated by the mixture of ammonia/nitrogen at 100 °C for 30 min. Then, to remove physisorbed ammonia, the catalyst was purged with a stream of nitrogen at the same conditions. After that, an NH₃-TPD curve was obtained by increasing the temperature up to 700 °C at a rate of 10°/min.

Temperature-programmed reduction (H₂-TPR) and temperature-programmed oxidation (TPO) experiments were carried out by using an STA 409 PC Luxx derivatograph (Netzsch, Germany) connected with a QMS-200 mass spectrometer (Pfeiffer Vacuum, Asslar, Germany). Before H₂-TPR experiments, the catalyst was held at 300 °C in a stream of N₂ for 1 h. For H₂-TPR, the samples (~50 mg) were heated from room temperature to 500 °C (5 °C/min) in a 10 vol.% H₂-Ar mixture with flow rate of 80 mL/min. For TPO, there were

no additional pretreatments of catalyst. The sample was heated from room temperature to 800 °C in a 10 vol.% O₂-Ar mixture with a flow rate of 80 mL/min.

X-ray structural analysis (XRD) of the catalysts was recorded on a Bruker D8 Advance diffractometer (CuK α radiation) (Bruker, Germany). The scan was performed in the 2 θ range of 8–63° with a step of 0.05° per 4 s. The analysis of the obtained diffraction data was carried out by using the program “PowderCell 2.4” with the JCPDS international diffraction database as a reference. Crystallite sizes were calculated by using the Scherrer equation.

CO₂ hydrogenation was carried out in a fixed-bed continuous flow stainless steel reactor at a 20–40 bar pressure, 200–300 °C temperature range, gas-hour space velocity (GHSV) = 12,000 h⁻¹ and inlet composition of H₂:CO₂ = 3:1. Before the experiments, all the catalysts (particle size 0.5–1 mm) were reduced at 300 °C for 1 h using a mixture of 10 vol.% H₂ in Ar. After that, the temperature was lowered to 200 °C, and the reaction mixture was fed on the catalyst. In most cases, the experiment was carried out for 8–10 h and 1 h before the pre-reduction of catalyst. The compositions of the inlet and outlet gas mixtures were identified by gas chromatography (GC Chromos-1000, Russia) with TCD and FID detectors and Porapak T/CaA columns. Catalytic activity was characterized by CO₂ conversion (%), DME and methanol (MeOH) selectivity (%) and DME production rate (g_{DME}/g_{cat}·h).

The detection limits for CO, CO₂, CH₄, DME and methanol were 5 × 10⁻³ vol.%. The carbon imbalance in all catalytic experiments was ±5%.

CO₂ conversion (X_{CO_2}), MeOH and DME selectivity (S_{MeOH} , S_{DME}) were calculated as follows:

$$X_{CO_2}(\%) = \frac{C_{CO} + C_{CH_4} + C_{MeOH} + 2 \times C_{DME}}{C_{CO} + C_{CH_4} + C_{MeOH} + 2 \times C_{DME} + C_{CO_2}} * 100 \quad (4)$$

$$S_{MeOH}(\%) = \frac{C_{MeOH}}{C_{CO} + C_{CH_4} + C_{MeOH} + 2 \times C_{DME}} * 100 \quad (5)$$

$$S_{DME}(\%) = \frac{2 * C_{DME}}{C_{CO} + C_{CH_4} + C_{MeOH} + 2 \times C_{DME}} * 100 \quad (6)$$

$$W_{DME} \left(\frac{g_{DME}}{h * g_{cat}} \right) = \frac{F_{DME} * M_{DME}}{m_{cat}} \quad (7)$$

where C_i^0 and C_i are the inlet and outlet concentrations (vol.%); F_i represents the flow rate (mol/h); n_i represents mole amount (mol); m represents catalyst weight (g); and M_i represents molecular weight (g/mol).

4. Conclusions

CuO/HNT and CuO-In₂O₃/HNT catalysts were studied in CO₂ hydrogenation to dimethyl ethers. With the help of physicochemical methods, such as TEM, XRD, S_{BET} , NH₃-TPD and H₂-TPR, we can suggest that copper-indium catalysts have two types of active sites: metallic copper mixed with indium oxide particles for methanol synthesis and halloysite acid sites for methanol dehydration to DME. CuO-In₂O₃/HNT provided 7.6% CO₂ conversion with 65% DME selectivity at 40 atm, T = 250 °C, GHSV = 12,000 h⁻¹ and inlet composition of H₂:CO₂ = 3:1, and it was stable after 10 h of experiment.

Supplementary Materials: The following are available online at <https://www.mdpi.com/article/10.3390/catal11101151/s1>, Figure S1: Nitrogen adsorption/desorption isotherms (A) and pore size distribution (B) of CuO-In₂O₃/HNT catalyst, Figure S2. SEM image of HNT, Figure S3. TEM image of HNT.

Author Contributions: Conceptualization, A.P., D.P. and A.G.; methodology, A.P., P.P. and M.R.; investigation, A.P.; writing—original draft preparation, A.P.; writing—review and editing, A.P., P.S., A.G. and D.P.; visualization, A.P. and M.R.; supervision, P.S. All authors have read and agreed to the published version of the manuscript.

Funding: This research was funded by RFBR project 19-33-60056.

Conflicts of Interest: The authors declare no conflict of interest.

References

1. Federsel, C.; Jackstell, R.; Beller, M. State-of-the-art catalysts for hydrogenation of carbon dioxide. *Angew. Chem. Int. Ed.* **2010**, *49*, 6254–6257. [[CrossRef](#)]
2. Shikada, T.; Ohno, Y.; Ogawa, T.; Ono, M.; Mizuguchi, M.; Tomura, K.; Fujimoto, K. Direct synthesis of dimethyl ether from synthesis gas. *Stud. Surf. Sci. Catal.* **1998**, *119*, 515–520.
3. Azizi, Z.; Rezaeimanesh, M.; Tohidian, T.; Rahimpour, M.R. Dimethyl ether: A review of technologies and production challenges. *Chem. Eng. Process. Intensif.* **2014**, *82*, 150–172. [[CrossRef](#)]
4. Catizzone, E.; Bonura, G.; Migliori, M.; Frusteri, F.; Giordano, G. CO₂ recycling to dimethyl ether: State-of-the-art and perspectives. *Molecules* **2018**, *23*, 31. [[CrossRef](#)] [[PubMed](#)]
5. Sun, J.; Yang, G.; Yoneyama, Y.; Tsubaki, N. Catalysis chemistry of dimethyl ether synthesis. *ACS Catal.* **2014**, *4*, 3346–3356. [[CrossRef](#)]
6. California Environmental Protection Agency. *California Dimethyl Ether Multimedia Evaluation, Tier 1*; California Environmental Protection Agency: Sacramento, CA, USA, 2015.
7. Snytnikov, P.V.; Badmaev, S.D.; Volkova, G.G.; Potemkin, D.I.; Zyryanova, M.M.; Belyaev, V.D.; Sobyenin, V.A. Catalysts for hydrogen production in a multifuel processor by methanol, dimethyl ether and bioethanol steam reforming for fuel cell applications. *Int. J. Hydrog. Energy* **2012**, *37*, 16388–16396. [[CrossRef](#)]
8. Semelsberger, T.A.; Borup, R.L.; Greene, H.L. Dimethyl ether (DME) as an alternative fuel. *J. Power Sources* **2006**, *156*, 497–511. [[CrossRef](#)]
9. Kunkes, E.L.; Studt, F.; Abild-Pedersen, F.; Schlögl, R.; Behrens, M. Hydrogenation of CO₂ to methanol and CO on Cu/ZnO/Al₂O₃: Is there a common intermediate or not? *J. Catal.* **2015**, *328*, 43–48. [[CrossRef](#)]
10. Ye, J.; Liu, C.; Mei, D.; Ge, Q. Active oxygen vacancy site for methanol synthesis from CO₂ hydrogenation on In₂O₃ (110): A DFT study. *ACS Catal.* **2013**, *3*, 1296–1306. [[CrossRef](#)]
11. Sun, K.; Fan, Z.; Ye, J.; Yan, J.; Ge, Q.; Li, Y.; He, W.; Yang, W.; Liu, C.J. Hydrogenation of CO₂ to methanol over In₂O₃ catalyst. *J. CO₂ Util.* **2015**, *12*, 1–6. [[CrossRef](#)]
12. Martin, O.; Martín, A.J.; Mondelli, C.; Mitchell, S.; Segawa, T.F.; Hauer, R.; Drouilly, C.; Curulla-Ferré, D.; Pérez-Ramírez, J. Indium Oxide as A Superior Catalyst for Methanol Synthesis by CO₂ hydrogenation. *Angew. Chem. Int. Ed.* **2016**, *55*, 6261–6265. [[CrossRef](#)]
13. Chen, T.Y.; Cao, C.; Chen, T.B.; Ding, X.; Huang, H.; Shen, L.; Cao, X.; Zhu, M.; Xu, J.; Gao, J.; et al. Unraveling Highly Tunable Selectivity in CO₂ Hydrogenation over Bimetallic In-Zr Oxide Catalysts. *ACS Catal.* **2019**, *9*, 8785–8797. [[CrossRef](#)]
14. Rui, N.; Wang, Z.; Sun, K.; Ye, J.; Ge, Q.; Liu, C.J. CO₂ hydrogenation to methanol over Pd/In₂O₃: Effects of Pd and oxygen vacancy. *Appl. Catal. B Environ.* **2017**, *218*, 488–497. [[CrossRef](#)]
15. Frei, M.S.; Capdevila-Cortada, M.; García-Muelas, R.; Mondelli, C.; López, N.; Stewart, J.A.; Curulla Ferré, D.; Pérez-Ramírez, J. Mechanism and microkinetics of methanol synthesis via CO₂ hydrogenation on indium oxide. *J. Catal.* **2018**, *361*, 313–321. [[CrossRef](#)]
16. Schack, C.J.; McNeil, M.A.; Rinker, R.G. Methanol synthesis from hydrogen, carbon monoxide, and carbon dioxide over a CuO/ZnO/Al₂O₃ catalyst: I. Steady-state kinetics experiments. *Appl. Catal.* **1989**, *50*, 247–263. [[CrossRef](#)]
17. Jadhav, S.G.; Vaidya, P.D.; Bhanage, B.M.; Joshi, J.B. Catalytic carbon dioxide hydrogenation to methanol: A review of recent studies. *Chem. Eng. Res. Des.* **2014**, *92*, 2557–2567. [[CrossRef](#)]
18. Ren, S.; Fan, X.; Shang, Z.; Shoemaker, W.R.; Ma, L.; Wu, T.; Li, S.; Kinghoffer, N.B.; Yu, M.; Liang, X. Enhanced catalytic performance of Zr modified CuO/ZnO/Al₂O₃ catalyst for methanol and DME synthesis via CO₂ hydrogenation. *J. CO₂ Util.* **2020**, *36*, 82–95. [[CrossRef](#)]
19. Naik, S.P.; Ryu, T.; Bui, V.; Miller, J.D.; Drinnan, N.B.; Zmierzczak, W. Synthesis of DME from CO₂/H₂ gas mixture. *Chem. Eng. J.* **2011**, *167*, 362–368. [[CrossRef](#)]
20. Bonura, G.; Cannilla, C.; Frusteri, L.; Mezzapica, A.; Frusteri, F. DME production by CO₂ hydrogenation: Key factors affecting the behaviour of CuZnZr/ferrierite catalysts. *Catal. Today* **2017**, *281*, 337–344. [[CrossRef](#)]
21. Frusteri, F.; Bonura, G.; Cannilla, C.; Ferrante, G.D.; Aloise, A.; Catizzone, E.; Migliori, M.; Giordano, G. Stepwise tuning of metal-oxide and acid sites of CuZnZr-MFI hybrid catalysts for the direct DME synthesis by CO₂ hydrogenation. *Appl. Catal. B Environ.* **2015**, *176*, 522–531. [[CrossRef](#)]
22. Bonura, G.; Cannilla, C.; Frusteri, L.; Catizzone, E.; Todaro, S.; Migliori, M.; Giordano, G.; Frusteri, F. Interaction effects between CuO-ZnO-ZrO₂ methanol phase and zeolite surface affecting stability of hybrid systems during one-step CO₂ hydrogenation to DME. *Catal. Today* **2020**, *345*, 175–182. [[CrossRef](#)]
23. Shi, Z.; Tan, Q.; Wu, D. A novel Core-Shell structured CuIn@SiO₂ catalyst for CO₂ hydrogenation to methanol. *AIChE J.* **2019**, *65*, 1047–1058. [[CrossRef](#)]
24. Yao, L.; Shen, X.; Pan, Y.; Peng, Z. Synergy between active sites of Cu-In-Zr-O catalyst in CO₂ hydrogenation to methanol. *J. Catal.* **2019**, *372*, 74–85. [[CrossRef](#)]
25. Glotov, A.; Vutolkina, A.; Pimerzin, A.; Vinokurov, V.; Lvov, Y. Clay nanotube-metal core/shell catalysts for hydroprocesses. *Chem. Soc. Rev.* **2021**, *50*, 9240–9277. [[CrossRef](#)]
26. Glotov, A.; Vutolkina, A.; Pimerzin, A.; Nedolivko, V.; Zasyalov, G.; Stytsenko, V.; Karakhanov, E.; Vinokurov, V. Ruthenium catalysts templated on mesoporous MCM-41 type silica and natural clay nanotubes for hydrogenation of benzene to cyclohexane. *Catalysts* **2020**, *10*, 537. [[CrossRef](#)]

27. Sadjadi, S.; Akbari, M.; Léger, B.; Monflier, E.; Heravi, M.M. Eggplant-derived biochar-halloysite nanocomposite as supports of Pd nanoparticles for the catalytic hydrogenation of nitroarenes in the presence of cyclodextrin. *ACS Sustain. Chem. Eng.* **2019**, *7*, 6720–6731. [[CrossRef](#)]
28. Sanchez-Ballester, N.M.; Ramesh, G.V.; Tanabe, T.; Koudelkova, E.; Liu, J.; Shrestha, L.K.; Lvov, Y.; Hill, J.P.; Ariga, K.; Abe, H. Activated interiors of clay nanotubes for agglomeration-tolerant automotive exhaust remediation. *J. Mater. Chem. A* **2015**, *3*, 6614–6619. [[CrossRef](#)]
29. Lvov, Y.; DeVilliers, M.; Fakhrullin, R. The potential of halloysite tubule clay in drug delivery applications. *Expert Opin. Drug Deliv.* **2016**, *13*, 977–988. [[CrossRef](#)]
30. Lazzara, G.; Cavallaro, G.; Panchal, A.; Fakhrullin, R.; Stavitskaya, A.; Vinokurov, V.; Lvov, Y. An assembly of organic-inorganic composites using halloysite clay nanotubes. *Curr. Opin. Colloid Interface Sci.* **2018**, *35*, 42–50. [[CrossRef](#)]
31. Glotov, A.; Stavitskaya, A.; Novikov, A.; Semenov, A.; Ivanov, E.; Gushchin, P.; Darrat, Y.; Vinokurov, V.; Lvov, Y. Halloysite Based Core-Shell Nanosystems: Synthesis and Application. *Nanomater. Clay Miner.* **2019**, 203–256. [[CrossRef](#)]
32. Fujiwara, K.; Okuyama, K.; Pratsinis, S.E. Metal-support interactions in catalysts for environmental remediation. *Environ. Sci. Nano* **2017**, *4*, 2076–2092. [[CrossRef](#)]
33. Wilson, I.; Keeling, J. Global occurrence, geology and characteristics of tubular halloysite deposits. *Clay Miner.* **2016**, *51*, 309–324. [[CrossRef](#)]
34. Lvov, Y.; Wang, W.; Zhang, L.; Fakhrullin, R. Halloysite clay nanotubes for loading and sustained release of functional compounds. *Adv. Mater.* **2016**, *28*, 1227–1250. [[CrossRef](#)]
35. Glotov, A.; Levshakov, N.; Stavitskaya, A.; Artemova, M.; Gushchin, P.; Ivanov, E.; Vinokurov, V.; Lvov, Y. Templated self-assembly of ordered mesoporous silica on clay nanotubes. *Chem. Commun.* **2019**, *55*, 5507–5510. [[CrossRef](#)]
36. Joussein, E.; Petit, S.; Churchman, J.; Theng, B.; Righi, D.; Delvaux, B. Halloysite clay minerals—a review. *Clay Miner.* **2005**, *40*, 383–426. [[CrossRef](#)]
37. Khan, A.; Rahman, F. Study of microstructural and optical properties of nanocrystalline indium oxide: A transparent conducting oxide (TCO). *AIP Conf. Proc.* **2019**, *2115*, 030091.
38. Luo, M.F.; Fang, P.; He, M.; Xie, Y.L. In situ XRD, Raman, and TPR studies of CuO/Al₂O₃ catalysts for CO oxidation. *J. Mol. Catal. A Chem.* **2005**, *239*, 243–248. [[CrossRef](#)]
39. Twigg, M.V.; Spencer, M.S. Deactivation of copper metal catalysts for methanol decomposition, methanol steam reforming and methanol synthesis. *Top. Catal.* **2003**, *22*, 191–203. [[CrossRef](#)]
40. Yao, L.; Shen, X.; Pan, Y.; Peng, Z. Unravelling Proximity-Driven Synergetic Effect within CIZO–SAPO Bifunctional Catalyst for CO₂ Hydrogenation to DME. *Energy Fuels* **2020**, *34*, 8635–8643. [[CrossRef](#)]